Appl. Phys. B 50, 415–423 (1990)

Applied Physics B Photophysics and Laser Chemistry

Performance of a Ten-Liter Electron Avalanche-Discharge XeCl Laser Device

S. Bollanti, P. Di Lazzaro, F. Flora, G. Giordano, T. Hermsen*, T. Letardi, and C. E. Zheng**

ENEA, Dip. TIB., U.S. Fisica Applicata, C.R.E. Frascati, C.P. 65 I-00044 Frascati, Rome, Italy

Revised Version Received 26 October 1989/Accepted 3 November 1989

Abstract. This paper describes the laser performance of an X-ray preionized ten-liter volume, electron-avalanche discharge XeCl system, operated at dc charging voltages of up to 70 kV both with and without X-ray preionization. An output energy of more than 11 J uniformly distributed over a $(7 \times 10)\,cm^2$ spot size was achieved using a multichannel spark-gap as the main discharge switch. The discharge was also successfully operated in the switchless mode, yielding a 4.8 J output energy and a 0.9% efficiency. The time-resolved gain measurements provided information on the laser discharge evolution.

PACS: 42.55H, 42.60

The potential applications of discharge-pumped excimer lasers (e.g., material processing, photochemistry, X-ray production) have stimulated a world-wide effort in the last few years in scaling excimer discharge systems to large volumes.

Very high energy-per-pulse discharge XeCl lasers have recently been developed in the USSR [1] with ultraviolet preionization, and in Japan [2] and the USA [3] with X-ray preionization. A common characteristic of the aforementioned devices is the very high pumping discharge voltage ranging from 120 kV [1] up to 400 kV [2]. Moreover, the X-ray generator voltage of the systems reported in [2, 3] is larger than 150 kV.

Looking at a commercial large-volume excimer laser, it is clear that the very high-voltage operation of both the discharge and the X-ray electron gun is not suitable for a user-friendly device. In Sect. 1, we shall report an investigation into the possibility of obtaining a reasonable energy extraction from a ten-liter active volume XeCl laser working at a low discharge voltage level (of up to 70 kV) and at a reduced X-ray preionization dosage.

Among the various difficulties encountered in our work, the achievement of a reliable, low cost and long-life switch for transferring the electrically stored energy into the laser head remains a major obstacle in the optimization of the laser device. To circumvent this problem, we operated our large-volume system in the so-called "switchless mode", i.e., triggering the pumping discharge by X-ray preionizing pulses [4]. The experimental results are presented in Sect. 2.

Some output laser performances operating the ten-liter discharge without preionization are reported in Sect. 3.

We conclude in Sect. 4 with a summary.

1. Experimental System and Results

The laser apparatus consists of three major components: an X-ray preionizer, a laser chamber, and the power supply for laser discharge pumping. The cross section of the preionizer and the laser cell with its spark gap switched dc charging pumping circuit system is shown in Fig. 1.

The X-ray preionizer employed has been reported in detail elsewhere [5], and only a brief description is given here. The X-ray diode, located in a vacuum chamber ($\sim 10^{-5}$ Torr), consists of two plasma cathodes and two lead target anodes. Each plasma cathode

* ENEA Guest

** ENEA Guest on leave from the Shanghai Institute of Optics and Fine Mechanics, the Chinese Academy of Sciences, Shanghai, China

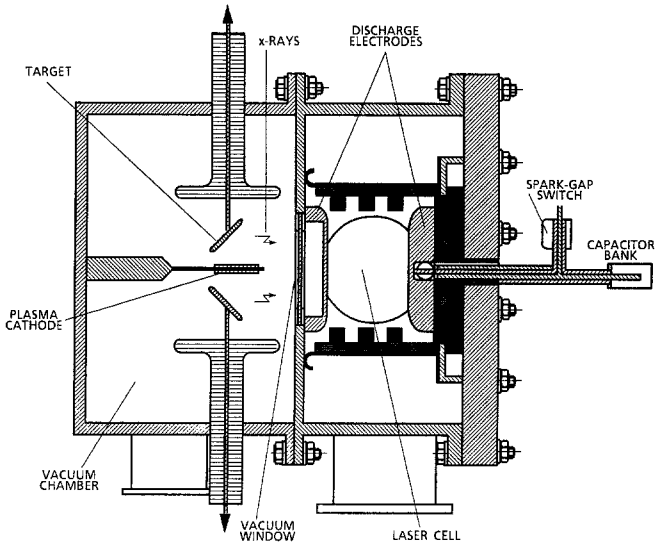

Fig. 1. Cross section of the X-ray preionized XeCl laser with dc charging pumping circuit

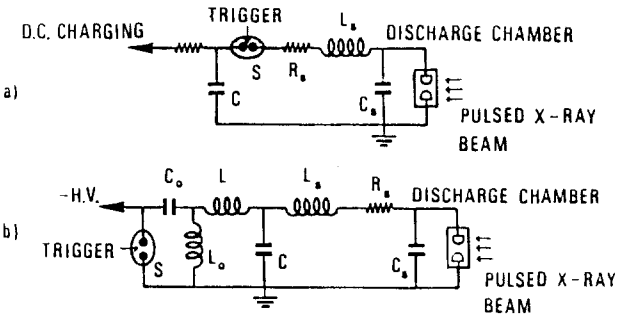

Fig. 2a, b. Schematic diagram of the discharge pumping circuit: **a** spark-gap switched pumping circuit; **b** resonant-charge-transfer-type excitation circuit. $C=0.64\ \mu F$; $C_0=1.3\ \mu F$. R_s and L_s are stray resistance and inductance, respectively. S is an eight-plug-triggered spark-gap switch, $C_s=2.3$ nF is a peaking capacitance

is at an angle of $\sim 45°$ to its corresponding anode, as shown in Fig. 1. The anodes of the X-ray diode are usually operated at a voltage of ~ 65 kV, produced by a resonant transformer with a stored energy of ~ 10 J in the capacitor of the secondary loop. When the high voltage pulse reaches its maximum value, the cathode plasma is triggered, and the plasma electrons driven by the applied high voltage pulse bombard the lead target anodes generating a beam of X-rays, 250 ns (FWHM) in duration, measured by a photomultiplier combined with a plastic scintillator. The X-ray beam leaving the anodes is transmitted through a 0.5-mm-thick aluminium window separating the vacuum chamber and the laser cell, then through a 0.5-mm-thick aluminium laser discharge cathode, and finally into the main discharge region.

The dosage measured in the discharge chamber was $\geqq 7$ mR. Under optimum operating conditions, the X-ray dosage was uniform to within 15% over the discharge length and to within 20% along the direction of the electric discharge field. Electric charge collection measurements, made by applying a dc field across the electrode gap, yielded an electron density of $\sim 1.5 \times 10^7/\text{cm}^3$ in one atmosphere of neon [5, 6].

The stainless steel laser cell has a total internal volume of ~ 200 l (Fig. 1). Two flat, fused silica windows, 16.5 cm in diameter and 2.5 cm in thickness, are mounted 240 cm apart. The electrodes are of a compact Stappaerts design [7], consisting of a shaped brass anode coated with nickel and a 0.5-mm-thick aluminium ground cathode pressed tightly onto a contoured aluminium block hollowed out to make the passage of the preionizing X-rays easier. On the aluminium ground cathode there is an array of sharp protrusions, ~ 0.5 mm high and ~ 0.4 cm apart from each other.

The electrodes were designed and processed for a nominal discharge width of 10 cm and a length of 100 cm at an electrode separation of 10 cm. The anode is connected by a 60-cm-wide brass plate to the discharge pumping circuit.

Two kinds of pumping circuits, shown in Fig. 2a and b, were tested in our experiments. The main discharge capacitor bank C consists of eight oil-and-paper capacitors in parallel ($8 \times 0.08\ \mu F/100$ kV, catalogue no. 31190, Maxwell Laboratories, Inc. USA), charged by a constant power, 10 kJ/s, KCC EL.EN. power supply.

An unoptimized plano-plano laser optical cavity was used in the experiments. The rear reflector was an aluminium-coated plane mirror, and the laser output coupler consisted of an uncoated silica in conjunction with one of the discharge chamber windows, with nominal reflectivities of 87% and 14% respectively, at $\lambda = 308$ nm laser wavelength emission. The laser mixture composition used in the discharge was HCl/Xe/Ne = 0.66/4.4/1000.

Figure 3a plots the time-resolved voltage-current characteristics for a typical discharge recorded using a Tektronix 2430 digital oscilloscope. The discharge power waveform, obtained by multiplying the discharge voltage $V(t)$ by the current $I(t)$, and the laser intensity waveform are shown in Fig. 3b. The discharge voltage was measured with a resistive divider, whilst the discharge current with a low-inductance strip shunt situated on the ground return circuit and made from a stainless steel foil with 2 mΩ resistance. The preionization was usually initiated in the discharge region, just about 0.3 μs before the high voltage was applied to the electrodes. When the delay time between the current peak of the X-ray diode and the onset of the discharge voltage was within ~ 0.4 μs, the laser output energy was almost constant.

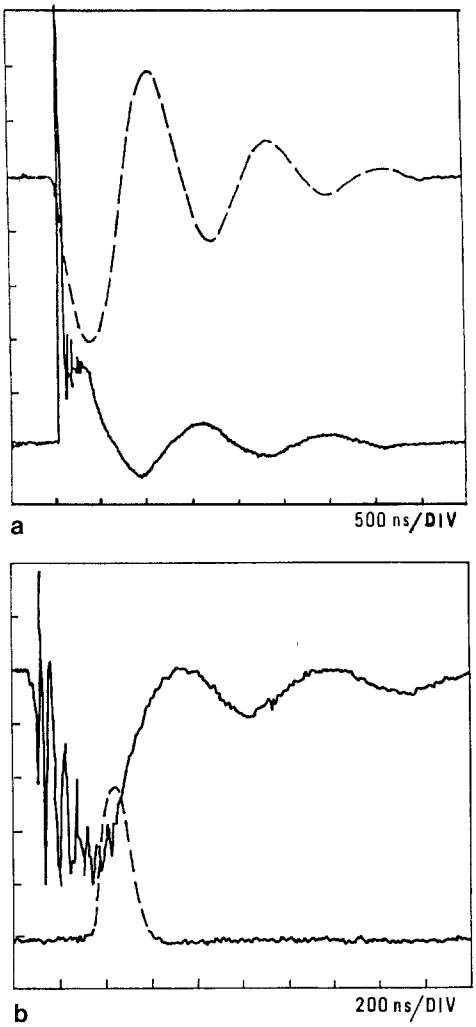

Fig. 3. a Time histories of the discharge voltage waveform (solid line) and current waveform (dashed line). Calibration 8.8 kV/div for voltage, 40 kA/div for current. **b** Time-resolved discharge power waveform (solid line) and laser intensity waveform (dashed line). 450 MW/div for power. Arbitrary units for laser intensity. Discharge capacitance $C=0.64\,\mu F$. Charging voltage: $V_0=55$ kV. Laser mixture pressure 3 atm

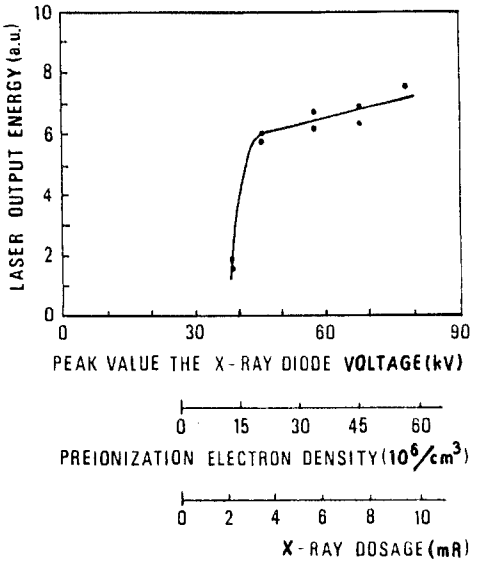

Fig. 4. Laser output energy vs preionization parameters. Plasma trigger voltage: 36 kV. Discharge capacitance: 0.48 μF. Charging voltage: 50 kV. The preionization electron number density scale refers to 3 atm of Ne

In order to increase the preionization effect, a peaking capacitance C_s in combination with a stray inductance L_s was introduced to establish an extremely high leading voltage pulse at the very beginning of the discharge (see Fig. 3a). When the X-ray dosage measured in the laser cell was lower than ~4 mR, the laser output energy was observed to be critically dependent on the X-ray intensity, as shown in Fig. 4. In the dosage range of over 4 mR, the increase of the laser output energy with the X-ray intensity was very slow. Although the preionization electron density shown in the scale of Fig. 4 was determined in neon, according to [8] it should be of the same order in a typical Ne-based XeCl laser mixture.

The discharge current rise time required for the current to rise from 10% to 90% of its peak values was about 210 ns, mainly depending on the total inductance L of ~70 nH and on the 0.64 μF capacitance C housed in the discharge circuit. Measurements show that the inductances of the discharge chamber and spark gap switch were $L_L=(9\pm3)$ nH and $L_s=(13\pm6)$ nH respectively, and the remainder of L was attributed to the capacitor bank and to electrical connections.

After the discharge voltage reached the steady state, as shown in Fig. 3a, the average electric field per unit pressure across the electrodes was ~0.4 kV/(cm atm.). Although the time duration Δt for which the steady state condition was observed was ~200 ns, the measured laser pulse duration was only 120 ns (FWHM) long and appeared to slowly increase with the discharge pumping energy. This premature termination of lasing can be due, in accordance with the experimental evidence on a similar, smaller volume system [9], to the plasma instabilities occurring during the steady state phase of the discharge.

Laser discharge characteristics were measured as a function of the discharge capacitance in the range of the dc charging voltage up to 70 kV. It was observed that for a given charging voltage V_0, the discharge energy dissipated into the active medium increased almost linearly with the discharge capacitance C. Figure 5 plots the ratio of the energy dissipated in the discharge chamber to the stored pumping energy as a function of the discharge capacitance. For the capacitance of 0.64 μF, about 60% of the electric

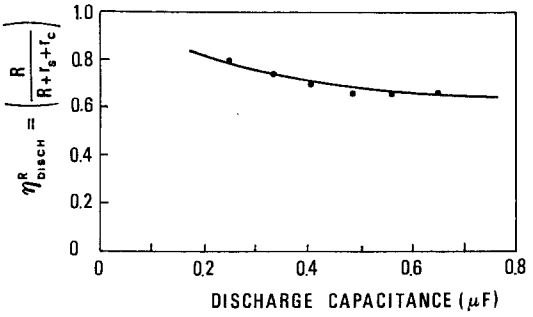

Fig. 5. Discharge efficiency $\eta^{R}_{discharge}$ vs discharge capacitance at a dc charging voltage $V_0 = 55$ kV, where R, r_s, and r_0 are the equivalent or average resistances of the gas discharge, the spark-gap switch, and the capacitor bank respectively, measured in the experiment

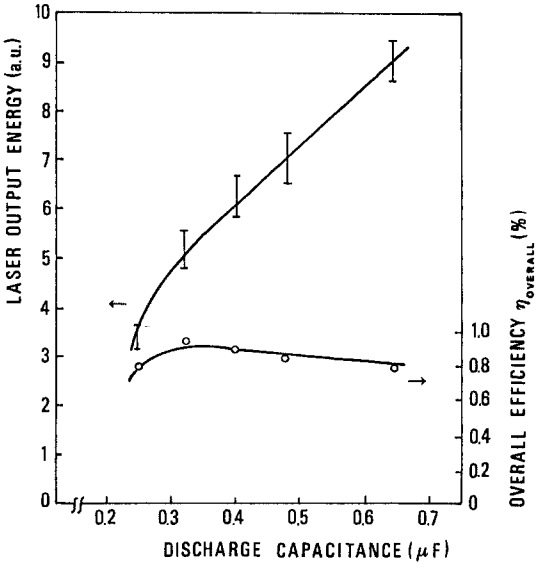

Fig. 6. Laser output energy and the corresponding overall efficiency $\eta_{overall}$ vs discharge capacitance. Charging voltage $V_0 = 50$ kV

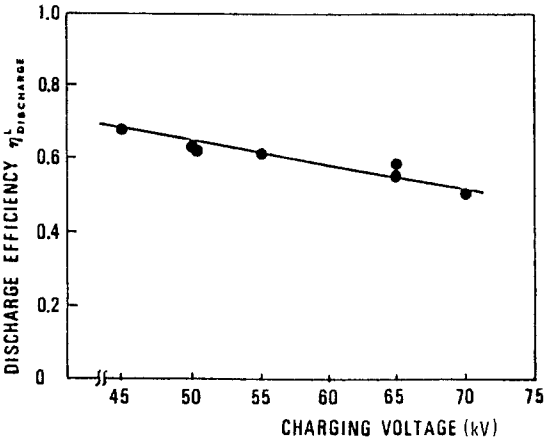

Fig. 7. Discharge efficiency $\eta^{L}_{discharge}$ as a function of the dc charging voltage, where

$$\eta^{L}_{discharge} = \frac{\int_0^{T_1} P(t)dt}{\int_0^{\infty} P(t)dt},$$

T_1 = first half oscillation period of the discharge power $P(t)$ dissipated in the 3 atm gas mixture

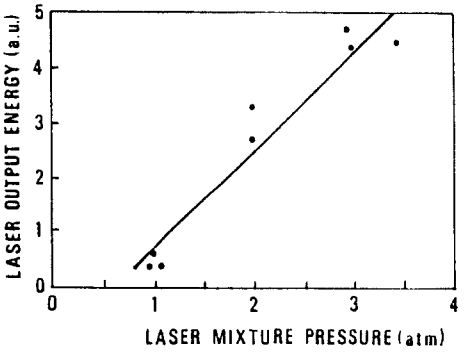

Fig. 8. XeCl laser output energy as a function of the gas mixture pressure. Discharge capacitance: 0.48 μF. Charging voltage: 50 kV

energy stored in the capacitor bank was deposited in the discharge.

Figure 6 shows the laser output energy and the corresponding overall efficiency $\eta_{overall}$ as a function of the discharge capacitance, where $\eta_{overall}$ is the ratio of the laser output energy to the electric stored energy. It can be seen that in the measured range of the discharge capacitance, the laser output energy is approximately linear with the capacitance, and then the overall laser efficiency remains almost constant.

Laser performance was then examined as a function of the dc charging voltage of the capacitor bank. In Fig. 7 we show the discharge efficiency $\eta^{L}_{discharge}$ as a function of the dc charging voltage V_0, where $\eta^{L}_{discharge}$ is defined as the ratio of the energy, dissipated in the gas mixture during the first half oscillation period of the discharge power, to the total discharge energy, i.e.,

$$\eta^{L}_{discharge} = \frac{\int_0^{T_1} I(t)V(t)dt}{\int_0^{\infty} I(t)V(t)dt}.$$

Strictly speaking, the real discharge power dissipated in the gas mixture is

$$P(t) = I(t)\left[V(t) - L_L \frac{dI}{dt}\right].$$

However, numerical simulation shows that this correction becomes negligible after the integration of $P(t)$ over the $(0\text{–}T_1)$ period. The weak dependence of $\eta^{L}_{discharge}$ on the dc charging voltage V_0 (Fig. 7) may be

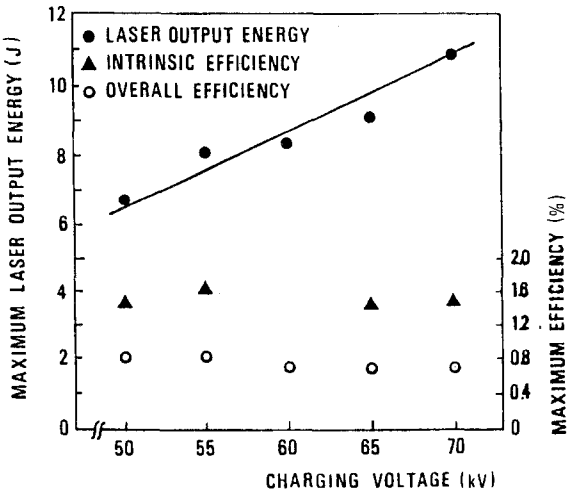

Fig. 9. Maximum laser output energy and corresponding maximum intrinsic and overall efficiencies as a function of the dc charging voltage. Discharge capacitance: 0.64 μF

due to the mismatch between the discharge chamber and pumping circuit impedances as the discharge resistance is smaller for higher V_0.

The asymptotic resistance of the discharge chamber, determined at 50 kV of the dc charging voltage during the lasing period, was $(55 \pm 5)\,\mathrm{m\Omega}$ and is much smaller than the output impedance of the discharge circuit which is 0.28 Ω estimated by $\sqrt{L_c/C}$; therefore, it may be expected that, for a given dc charging voltage, the laser output energy should increase with the gas mixture pressure since the impedance match can be improved in this case, as shown in Fig. 8.

Figure 9 shows the maximum laser output energy, the corresponding intrinsic efficiency $\eta_{\text{intrinsic}}$, and the overall efficiency vs the dc charging voltage, where

$$\eta_{\text{intrinsic}} = \frac{\text{laser output energy}}{\int_0^{T_1} I(t)V(t)dt}.$$

The near-field laser spatial profile was examined by means of a fluorescent target and a video digital system composed of a standard TV camera, an 8-bit A/D converter, and a 128 Kbyte frame memory [10]. In this experiment, a sheet of Xerox copy paper was used as the target. Before irradiating the paper, the laser beam intensity was properly attenuated so that the resultant fluorescence intensity was linear with the laser intensity [11]. Although a discharge area of $10 \times 10\,\mathrm{cm}^2$ was designed, a laser spot area of only $10 \times 7\,\mathrm{cm}^2$ was obtained due to the inhomogeneity in the discharge volume near the cathode [1, 9]. Figure 10 gives the laser intensity distribution measured in the near field.

In order to have a better assessment of the active medium potentiality, and also for modelling purposes,

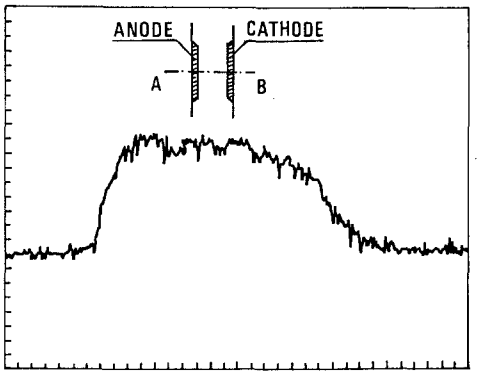

Fig. 10. Laser intensity distribution along A–B direction in the near-field. The FWHM is 7 cm

some time-resolved gain measurements were made using the mode selected output of a Lambda Physics EMG50 XeCl laser operated with a positive branch unstable resonator. The 14 ns (FWHM) probe pulse was monitored both before and after entering the laser discharge region using ITT FW114 vacuum photodiodes, equipped with S-20-type photocathodes. Neutral density filters were placed both in front of each photodiode and at the entrance of the XeCl discharge in order to ensure that the detector working point was far away from saturation and that the gain was in the linear region. A spatial filter ($\theta \sim 10$ times the diffraction limit, placed behind the laser cell, increased the signal-to-noise ratio, allowing a cut-off of the XeCl fluorescence background noise. Timing of the probe pulse with respect to the discharge waveforms was monitored with a Tektronix 2430 digital oscilloscope. The reference and amplified probe pulse were acquired using a Tektronix 7912AD Programmable Digitizer, interfaced with a Hewlett Packard 9000 model 310 computer.

Figure 11 plots the time behavior of the measured net gain on the optical axis, at the center of the

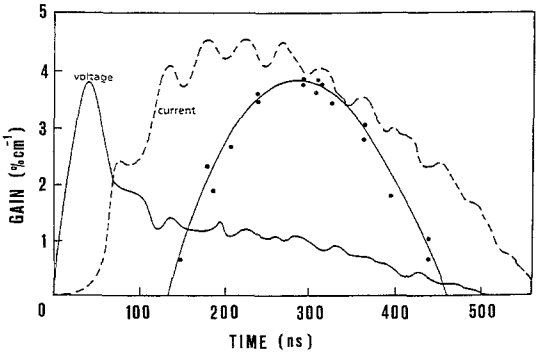

Fig. 11. Temporal evolution of the net small signal gain (solid points), discharge current (dashed line), and voltage (solid line). The discharge current and voltage are in arbitrary units. Averaged power density deposition $75\,\mathrm{kW/cm^3}$. $C = 0.64\,\mu\mathrm{F}$, $V_0 = 55\,\mathrm{kV}$

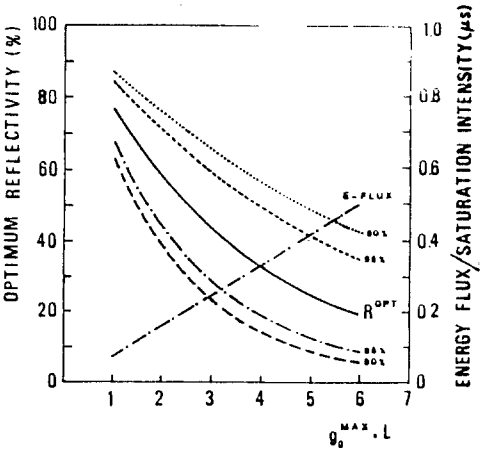

Fig. 12. Optimum reflectivity R^{opt} and normalized energy flux (straight line) for a plano-plano cavity. (See text)

discharge. The current and voltage waveforms are also shown for reference. The small signal gain raised after the applied field reached the self-sustaining region, where $E/N \sim 1.6 \times 10^{-17}$ V · cm^2. The peak value of $(g_0 - \alpha)^{max} = 4\%$ cm^{-1} occurred ~ 100 ns delayed against the current maximum, and significant gain was observed for low values of power deposition.

These results have been used to simulate the intracavity photon flux evolution in a plano-plano resonator as a function of the output mirror reflectivity. In the model, the quasi-stationary Rigrod equations for counterpropagating intensities inside the active medium were employed and a ratio $\gamma = 10$ of the gain coefficient to the absorption coefficient was assumed to be constant in time, as indicated by previous measurements [12]. The results are shown in Fig. 12. Here, the 90% and 95% curves indicate reflectivities for which the extracted energy is 90% and 95% of the optimum value, respectively, for a given peak value of the coefficient $g_0 L$. The curve "e-flux" gives the energy flux normalized to the saturation intensity in MW/cm^2 (using the right-hand scale) for the corresponding optimum mirror reflectivity. From Figs. 11 and 12, a maximum laser energy of about 15 J may be achieved using an output coupler mirror with a reflection coefficient of $\sim 30\%$ and assuming a saturation intensity of 0.8 MW/cm^2 [12].

2. X-Ray Triggered Discharge

In order to circumvent the topical problem of having a reliable switching in the main laser discharge circuit, a phototriggering technique has recently been proposed [4]. It consists of creating the preionization electron density after the establishment of the discharge voltage across the main discharge electrodes. In practice, the energy storage device is directly connected with the laser head, and the applied voltage is slowly raised up to slightly less than the self-breakdown voltage. A pulse of ionizing radiation is then injected into the gas mixture, providing the avalanche process development. When the discharge impedance becomes comparable to that of the external circuit, efficient transfer of pumping energy occurs, thus leading to pulse laser emission.

In particular, the initiation of a high pressure laser discharge by X-rays allowed a substantial circuital simplification, even if successful operations were limited to a maximum discharge volume of about one liter [13, 14].

Using the circuit shown in Fig. 2b, the laser characteristics of the X-ray-initiated discharge were measured as a function of the charging voltage, the gas pressure, and the X-ray dosage. In all these experiments, the output energy increased with the above-mentioned variables without any sign of saturation. However, the charging voltage was limited by the self-breakdown level of the gas mixture, which mainly depends on the total gas pressure, for a given composition. In our device, mechanical constraints limited the maximum gas pressure to 3.5 atm, so we finally increased the X-ray dosage level by increasing the energy stored in the secondary loop of the resonant transformer of the preionizer. The remainder of the preionizer system (Sect. 1) was left unchanged. In this way, 37 J stored energy allowed a 18 mR X-ray dosage and 3.3×10^7 cm^{-3} electron-ion pairs in the laser chamber, measured with Physiotechnie SEQ5 pen dosimeters and electric charge collection in 1 atm Ne, respectively.

Figure 13 plots the laser output energy vs the X-ray dosage used for the discharge triggering. The working point was 3 atm gas mixture, 31 kV discharge voltage, 14% output coupler reflection coefficient. Here, both low and high stored energy preionizer results have been reported, and the laser output energy is clearly more sensitive to the X-ray dosage than in the spark-gap triggered discharge case (cf. Figs. 4 and 13). The near-field laser burn pattern was recorded on Dylux UV sensitive paper, showing a very uniform distribution. The burn dimensions were (6×9) cm^2, about 20% less than the spot size obtained with the conventionally triggered discharge.

Moreover, Fig. 13 does not show clear saturation effects, and a higher output energy can be expected, working at a larger preionization density level.

In our case, however, the main energy scaling limitation was determined by the self-breakdown level of the gas mixture, which prevented us from reliably working at a discharge voltage higher than 31 kV. We therefore increased the gas mixture pressure up to 3.5 atm, just adding 0.5 atm of Ne to the usual mixture.

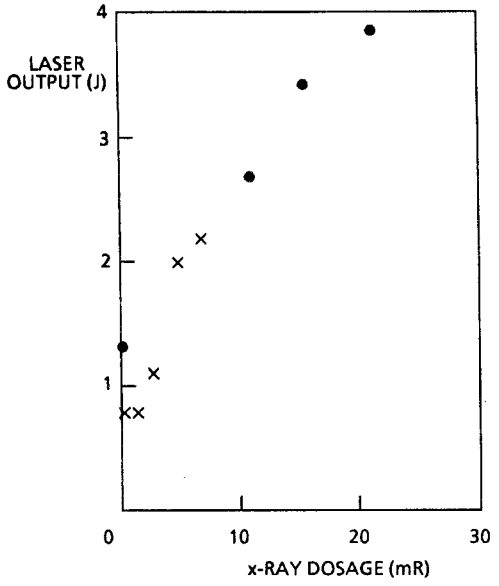

Fig. 13. Laser output energy vs X-ray dosage for the discharge triggered by X-rays, for a laser gas mixture pressure of 3 atm and a discharge voltage $V_0 = 31$ kV. Crossed points are relative to the 10 J preionizer described in [5]. Solid points were obtained using a higher stored energy preionizer

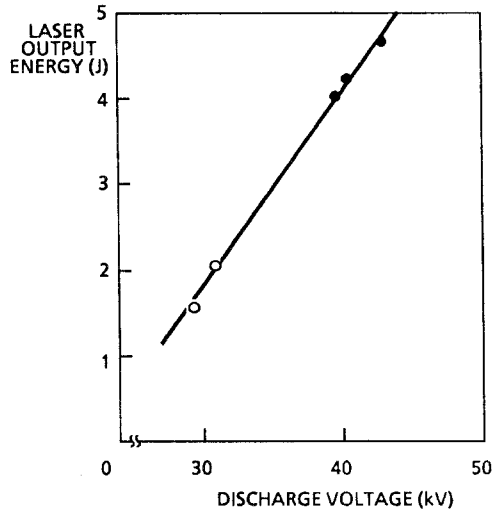

Fig. 14. Laser output energy vs discharge voltage for the X-ray triggered discharge. Solid points: 3.5 atm gas pressure, composition HCl : Xe : Ne = (0.56 : 3.8 : 1000). Open points: 3 atm gas pressure, composition HCl : Xe : Ne = (0.66 : 4.4 : 1000)

The result is shown in Fig. 14 where the output laser energy is plotted as a function of the discharge voltage. A maximum laser output energy of 4.8 J was obtained at a discharge voltage of 41 kV, with an associated overall efficiency of 0.9%, of the same order as that achieved with the spark-gap triggered discharge (see Fig. 9).

Decreasing the gas mixture pressure, we observed laser output up to 1.5 atm, without changing the near-field spot size and uniformity. The results are plotted in

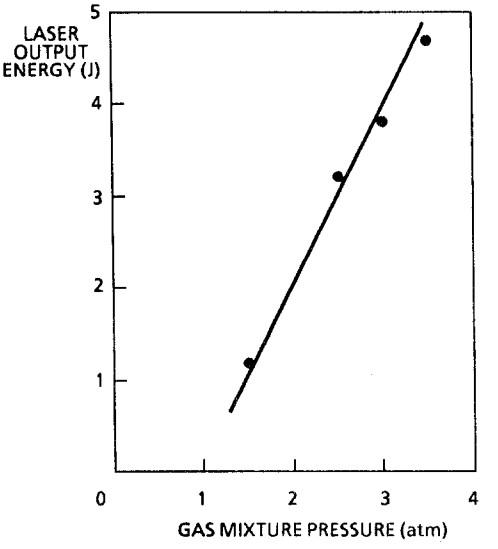

Fig. 15. Laser output energy vs gas mixture pressure for the X-ray triggered discharge. Composition HCl : Xe : Ne = (0.56 : 3.8 : 1000)

Fig. 15. In this experiment, however, the E/p working point at the beginning of the discharge was not exactly constant, ranging from 1.2 kV/(cm · atm) for the 3.5 atm gas pressure, up to 1.5 kV/(cm · atm) for the 1.5 atm gas pressure.

3. Laser Discharge Without X-Ray Preionization

Using the resonant-charge-transfer-type excitation circuit shown in Fig. 2b, the laser discharge performances have been studied for the case without X-ray preionization. As a matter of fact, from Fig. 13, it can be seen that even when the X-ray intensity was reduced to zero, there was still a laser output energy of (0.8–1.3) J, with a laser spot size of $(7 \times 2)\,\text{cm}^2$ in the near field. The attainment of the fairly uniform discharge is related to the preionization of the corona developed near the cathode sharp protrusions at the very beginning of the discharge.

The application of this kind of cathode geometry for obtaining pulsed high pressure laser discharges can be traced back to more than 15 years ago [15]. In this paper, we only give a description of some experimental results obtained in our laboratory, and the details to this discharge process will be discussed further in another paper.

Figure 16 shows the laser output vs the dc charging voltage for laser gas mixture pressures of 3 and 1.5 atm. In these measurements, the rise time for the discharge voltage was about 1 μs. Typical discharge voltage, discharge current, and laser intensity waveforms are

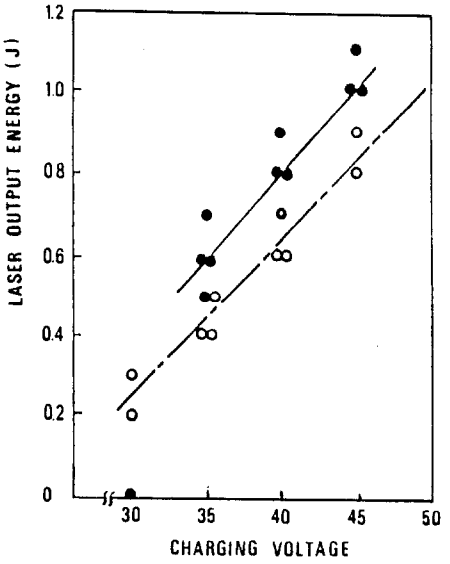

Fig. 16. Laser output energy vs charging voltage without X-ray preionization. ● Laser gas mixture pressure 3 atm; ○ Laser gas mixture pressure 1.5 atm

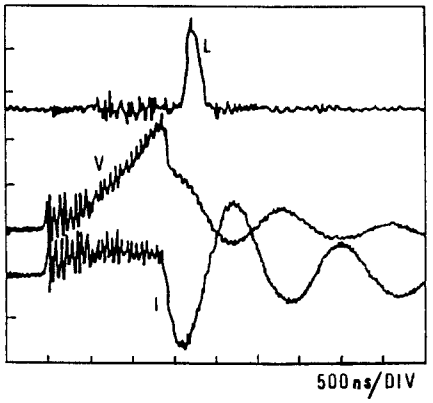

Fig. 17. Time-resolved discharge voltage (V), discharge current (I), and laser intensity (L) waveforms at a charging voltage $V_0 = 45$ kV, and laser gas mixture pressure 1.5 atm, obtained without X-ray preionization. The vertical scales are in arbitrary units

shown in Fig. 17. An interesting point is that when the full width of the rise time for the discharge voltage was as short as 10–20 ns, as in the case using the spark-gap switched pumping circuit (Fig. 3a), we could not obtain laser output without X-ray preionization (see Fig. 4).

The laser pulse durations (FWHM) of ~120 ns were observed to be almost the same as for the previously described experiments.

4. Summary

In this paper we have investigated the laser output energy and discharge performances for a ten-liter active volume, avalanche discharge XeCl laser as a function of various parameters.

Commercial paper-and-oil capacitors were used for the laser discharge pumping because they are more compact than a water transmission line pumping system.

The laser discharge performances were mainly studied at a voltage level lower than 70 kV, which is convenient for the extension to the repetition-rate mode operation.

Using the spark-gap switched XeCl discharge with X-ray preionization (Fig. 2a), 11 J of output energy uniformly distributed on a $(7 \times 10)\,\mathrm{cm}^2$ near-field spot size were extracted from a 3 atm, Ne-based mixture at a dc charging voltage of 70 kV with an unoptimized optical cavity. The delayed onset of the output laser emission with respect to the discharge pumping power (Fig. 3) and the relatively low value of the net gain (Fig. 11) suggest reducing the optical cavity losses. The numerical simulation results (Fig. 12) confirm the possibility of being able to achieve a 30% increment in the laser output energy when dielectric coated mirrors with optimum reflectivity are available.

Various efficiencies (η_{overall}, $\eta_{\mathrm{intrinsic}}$, $\eta^{\mathrm{L}}_{\mathrm{discharge}}$, and $\eta^{\mathrm{R}}_{\mathrm{discharge}}$) were measured to get a better understanding of where the input energy was dissipated or allotted during the discharge period.

Using the resonant-charge-transfer-type excitation circuit (Fig. 2b), the full width of the rise time for the discharge voltage was as long as ~1 μs. When the X-rays were used for the trigger of the discharge, it was found that for a dosage level over 4 mR, the increase of the laser output energy with the X-ray intensity was much more sensitive to the X-ray dosage than for the case of the spark-gap switched discharge.

To our knowledge, this is the first successful operation of a large-volume, discharge pumped laser device using a switchless technique, and the 4.8 J output energy obtained is the highest reported with X-ray-triggered discharge excimer lasers.

Using the same excitation circuit and without X-ray preionization, about 1 J laser energy output was achieved.

These results need further theoretical and experimental investigation to make the self-switching technique competitive with the conventionally switched discharge system. This effort would be justified by the obvious potential of the technique in terms of circuit simplicity and laser compactness, making it a promising option for long pulse, high repetition rate excimer lasers and, in particular, for relatively slow avalanche-process-time active media such as XeCl [13].

In conclusion, we believe that the XeCl laser device outlined is a promising prototype for a commercial, large-volume XeCl laser operating both at 10 J output

energy, low repetition rate (1–10 Hz) and at 5 J, 20 Hz in the switchless mode. This system, in the final version, could open interesting prospects in the area of materials processing and metal shock-hardening [16].

References

1. V.Yu. Baranov, V.M. Borisov, D.N. Molchanov, V.P. Novikov, O.B. Khritoforov: Sov. J. Quantum Electron. **17**, 978 (1987)
2. T. Hasama, K. Miyazaki, K. Yamada, K. Ohuchi, T. Sato: J. Appl. Phys. **61**, 4691 (1987)
   T. Hasama, K. Miyazaki, K. Yamada, T. Sato: IEEE J. QE-**25**, 113 (1988)
3. L.F. Champagne, A.J. Dudas, N.W. Harris: J. Appl. Phys. **62**, 1576 (1987)
4. J. Bretagne, Y. Louvet: J. Appl. Phys. **61**, 827 (1987)
5. T. Letardi, P. Di Lazzaro, G. Giordano, C.E. Zheng: Appl. Phys. B **48**, 55 (1989)
6. G. Giordano, T. Letardi, C.E. Zheng: Nuovo Cimento **101** B, 569 (1988)
7. E.A. Stappaerts: Appl. Phys. Lett. **40**, 1018 (1982)
8. C.E. Zheng, D. Lo: Chin. J. of Lasers **14**, 193 (1987)
   Shao-chi Lin, Cheng-En Zheng, Dennis Lo, J. Matsumoto, Sheng-Bai Zhu: Appl. Phys. B **40**, 15 (1986)
9. A. De Angelis, P. Di Lazzaro, F. Garosi, G. Giordano, T. Letardi: Appl. Phys. B **47**, 1 (1988)
10. V. Boffa, P. Di Lazzaro, G.P. Gallerano, G. Giordano, T. Hermsen, T. Letardi, C.E. Zheng: IEEE J. QE-**23**, 1241 (1987)
11. Despite the apparent roughness of the method, the use of uncalibrated fluorescent paper can offer enough resolution at low cost for wide aperture excimer lasers if the intensity measurement is carefully performed. See, e.g., Laser Focus, Vol. **25** (August 1989) p. 21
12. T. Letardi, V. Boffa, S. Bollanti, P. Di Lazzaro, G. Giordano, T. Hermsen, E. Sabia, C.E. Zheng: Nuovo Cimento **11**D, 1733 (1989)
13. B. Lacour, C. Vannier: J. Appl. Phys. **62**, 754 (1987)
14. K. Jayaram, A.J. Alcock: Appl. Phys. Lett. **46**, 636 (1985)
15. A.J. Bealieu: Appl. Phys. Lett. **16**, 504 (1970)
    K.A. Laurie, M.M. Hale: IEEE J. QE-**6**, 530 (1970)
16. S. Tosto, P. Di Lazzaro, T. Letardi, S. Marelli: *Metal Surface Treatments by Means of High Energy* UV *Laser Pulses*, Proc. ECO 1 Conf. on "Excimer Laser and Applications", SPIE Vol. 1023 (Hamburg 1988) p. 208